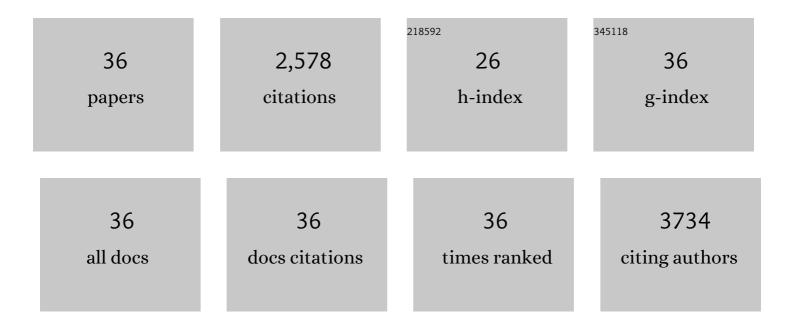
Xiao-Rong Song

List of Publications by Year in descending order

Source: https://exaly.com/author-pdf/231381/publications.pdf Version: 2024-02-01



#	Article	IF	CITATIONS
1	Near-Infrared II Gold Nanocluster Assemblies with Improved Luminescence and Biofate for In Vivo Ratiometric Imaging of H ₂ S. Analytical Chemistry, 2022, 94, 2641-2647.	3.2	51
2	A New Class of NIRâ€II Gold Nanoclusterâ€Based Protein Biolabels for Inâ€Vivo Tumorâ€Targeted Imaging. Angewandte Chemie, 2021, 133, 1326-1332.	1.6	14
3	An Activatable Xâ€Ray Scintillating Luminescent Nanoprobe for Early Diagnosis and Progression Monitoring of Thrombosis in Live Rat. Advanced Functional Materials, 2021, 31, 2006353.	7.8	22
4	A New Class of NIRâ€II Gold Nanoclusterâ€Based Protein Biolabels for Inâ€Vivo Tumorâ€Targeted Imaging. Angewandte Chemie - International Edition, 2021, 60, 1306-1312.	7.2	155
5	Engineered Nanoscale Vanadium Metallodrugs for Robust Tumor pecific Imaging and Therapy. Advanced Functional Materials, 2021, 31, 2010337.	7.8	22
6	High-resolution X-ray luminescence extension imaging. Nature, 2021, 590, 410-415.	13.7	378
7	Broadband Detection of Xâ€ray, Ultraviolet, and Nearâ€Infrared Photons using Solutionâ€Processed Perovskite–Lanthanide Nanotransducers. Advanced Materials, 2021, 33, e2101852.	11.1	51
8	Effects of hydroxyl radicals produced by a zinc phthalocyanine photosensitizer on tumor DNA. Dyes and Pigments, 2020, 173, 107894.	2.0	10
9	Broadband excitable NIR-II luminescent nano-bioprobes based on CuInSe2 quantum dots for the detection of circulating tumor cells. Nano Today, 2020, 35, 100943.	6.2	57
10	Light-Switchable Yolk–Mesoporous Shell UCNPs@MgSiO ₃ for Nitric Oxide-Evoked Multidrug Resistance Reversal in Cancer Therapy. ACS Applied Materials & Interfaces, 2020, 12, 30066-30076.	4.0	45
11	Near-infrared-excited upconversion photodynamic therapy of extensively drug-resistant <i>Acinetobacter baumannii</i> based on lanthanide nanoparticles. Nanoscale, 2020, 12, 13948-13957.	2.8	43
12	A series of photosensitizers with incremental positive electric charges for photodynamic antitumor therapy. RSC Advances, 2019, 9, 24560-24567.	1.7	6
13	Direct Detection of Circulating Tumor Cells in Whole Blood Using Timeâ€Resolved Luminescent Lanthanide Nanoprobes. Angewandte Chemie, 2019, 131, 12323-12327.	1.6	4
14	Direct Detection of Circulating Tumor Cells in Whole Blood Using Timeâ€Resolved Luminescent Lanthanide Nanoprobes. Angewandte Chemie - International Edition, 2019, 58, 12195-12199.	7.2	62
15	Grapheneâ€Oxideâ€Modified Lanthanide Nanoprobes for Tumorâ€Targeted Visible/NIRâ€II Luminescence Imaging Angewandte Chemie - International Edition, 2019, 58, 18981-18986.	7.2	92
16	Grapheneâ€Oxideâ€Modified Lanthanide Nanoprobes for Tumorâ€Targeted Visible/NIRâ€II Luminescence Imaging Angewandte Chemie, 2019, 131, 19157-19162.	1.6	12
17	<p>Tumor-targeting photodynamic therapy based on folate-modified polydopamine nanoparticles</p> . International Journal of Nanomedicine, 2019, Volume 14, 6799-6812.	3.3	32
18	Highly efficient luminescent I-III-VI semiconductor nanoprobes based on template-synthesized CuInS2 nanocrystals. Nano Research, 2019, 12, 1804-1809.	5.8	19

XIAO-RONG SONG

#	Article	IF	CITATIONS
19	Near-Infrared Light-Triggered Sulfur Dioxide Gas Therapy of Cancer. ACS Nano, 2019, 13, 2103-2113.	7.3	86
20	An efficient synergistic cancer therapy by integrating cell cycle inhibitor and photosensitizer into polydopamine nanoparticles. Journal of Materials Chemistry B, 2018, 6, 2620-2629.	2.9	16
21	Enhancing Antitumor Efficacy by Simultaneous ATPâ€Responsive Chemodrug Release and Cancer Cell Sensitization Based on a Smart Nanoagent. Advanced Science, 2018, 5, 1801201.	5.6	35
22	Large-scale synthesis of uniform lanthanide-doped NaREF ₄ upconversion/downshifting nanoprobes for bioapplications. Nanoscale, 2018, 10, 11477-11484.	2.8	84
23	Engineering of tungsten carbide nanoparticles for imaging-guided single 1,064 nm laser-activated dual-type photodynamic and photothermal therapy of cancer. Nano Research, 2018, 11, 4859-4873.	5.8	42
24	Repeatable deep-tissue activation of persistent luminescent nanoparticles by soft X-ray for high sensitivity long-term in vivo bioimaging. Nanoscale, 2017, 9, 2718-2722.	2.8	74
25	Polyphenolâ€Inspired Facile Construction of Smart Assemblies for ATP―and pHâ€Responsive Tumor MR/Optical Imaging and Photothermal Therapy. Small, 2017, 13, 1603997.	5.2	70
26	Plant Polyphenolâ€Assisted Green Synthesis of Hollow CoPt Alloy Nanoparticles for Dualâ€Modality Imaging Guided Photothermal Therapy. Small, 2016, 12, 1506-1513.	5.2	57
27	Functionalization of metal nanoclusters for biomedical applications. Analyst, The, 2016, 141, 3126-3140.	1.7	279
28	Enzyme-free amplified detection of microRNA using target-catalyzed hairpin assembly and magnesium ion-dependent deoxyribozyme. Science China Chemistry, 2015, 58, 1906-1911.	4.2	11
29	Co ₉ Se ₈ Nanoplates as a New Theranostic Platform for Photoacoustic/Magnetic Resonance Dualâ€Modalâ€Imagingâ€Guided Chemoâ€Photothermal Combination Therapy. Advanced Materials, 2015, 27, 3285-3291.	11.1	265
30	Topological insulator bismuth selenide as a theranostic platform for simultaneous cancer imaging and therapy. Scientific Reports, 2013, 3, 1998.	1.6	137
31	Nicking enzyme based homogeneous aptasensors for amplification detection of protein. Chemical Communications, 2012, 48, 374-376.	2.2	33
32	A graphene oxide (GO)-based molecular beacon for DNA-binding transcription factor detection. Nanoscale, 2012, 4, 3655.	2.8	44
33	Label-free and fluorescence turn-on aptasensor for protein detection via target-induced silver nanoclusters formation. Analytica Chimica Acta, 2012, 749, 70-74.	2.6	61
34	Enzyme-free fluorescence aptasensor for amplification detection of human thrombin via target-catalyzed hairpin assembly. Biosensors and Bioelectronics, 2012, 36, 217-221.	5.3	54
35	Enzyme-free signal amplification in the DNAzyme sensor via target-catalyzed hairpin assembly. Chemical Communications, 2012, 48, 3112.	2.2	128
36	Multiplex detection of nucleases by a graphene-based platform. Journal of Materials Chemistry, 2011, 21, 10915.	6.7	27